Optics Letters

Characterizing chromatin packing scaling in whole nuclei using interferometric microscopy

Aya Eid,[1] Adam Eshein,[1] Yue Li,[1] Ranya Virk,[1] David Van Derway,[1] Di Zhang,[1] Allen Taflove,[2] and Vadim Backman[1,*]

[1]Department of Biomedical Engineering, Northwestern University, Evanston, Illinois 60208, USA
[2]Department of Electrical Engineering, Northwestern University, Evanston, Illinois 60208, USA
*Corresponding author: v-backman@northwestern.edu

Received 18 June 2020; revised 21 July 2020; accepted 22 July 2020; posted 22 July 2020 (Doc. ID 400231); published 25 August 2020

Chromatin is the macromolecular assembly containing the cell's genetic information, and its architectural conformation facilitates accessibility to activation sites and thus gene expression. We have developed an analytical framework to quantify chromatin structure with spectral microscopy. Chromatin structure can be described as a mass fractal, with packing scaling D up to specific genomic length scales. Considering various system geometries, we established a model to measure D with the interferometric technique partial wave spectroscopy (PWS) and validated the analysis using finite difference time domain to simulate the PWS system. Calculations of D were consistent with ground truth electron microscopy measurements, enabling a high-throughput, label-free approach to quantifying chromatin structure in the nanometer length scale regime.

https://doi.org/10.1364/OL.400231

To enclose more than 2 m of human DNA within a nuclear diameter less than <10 μm and still allow for gene-specific accessibility, genomic DNA must fold into an organized, yet compact arrangement with varying length scales of packing structure. In the lowest order, DNA wraps around histone proteins forming 11 nm nucleosome complexes, recognized as the "beads on a string" structure. Above this level of organization, recent imaging studies have identified the primary *in situ* organization as disordered chains with diameters between 5 and 24 nm that pack together with varying volume concentration [1]. At a larger scale, chromatin is organized into packing domains (PDs) within which it adopts a power-law scaling relationship between the number of monomers (N_f), proportional to the polymer mass and the space it occupies (e.g., $N_f \propto r^D$) [2]. Within the power-law regime, chromatin packing behavior can be characterized packing scaling D [3]. This parameter gives insight into the physical structure of chromatin; for example, higher values of D describe increased packing with a shift in the mass-density distribution towards more heterogeneous structures. Additionally, the biological significance of D has been correlated with phenotypic plasticity, cancer staging, and large-scale gene expression patterns [4–6]. For length scales beyond a PD (∼6 kbp − ∼5 Mbp), chromatin is organized into chromosomal compartments associated by transcriptional activity; however, the interplay between PDs and large-scale chromatin organization is poorly understood [7].

While there is an increasing number of techniques to quantify chromatin structure, few can image with sufficient resolution while collecting significant statistics. A recent super resolution development using single nucleosome labeling has enabled live cell, dynamic imaging of chromatin structure with 20 nm resolution [8]. However, high irradiation technologies are known to induce phototoxicity and alter molecular structure.

Chromatin transmission electron microscopy (ChromTEM) uses bright-field TEM with DNA labeling to acquire 2D images of chromatin structure with nanometer resolution. Autocorrelation analysis on the chromatin mass-density distribution can unambiguously measure chromatin packing scaling D. Although considered a ground truth measurement of chromatin organization, ChromTEM is time intensive and does not allow for live-cell imaging.

Partial pave spectroscopy (PWS), on the other hand, is label free, has high throughput, and uses a relatively simple, microscopy system for 2D interference based live-cell imaging. It relies on a common-path reference at the cell–glass interface to amplify the backscattering spectrum from refractive index (RI) variations within a cell. From this signal, the spectral deviation Σ, can be computed for every $x - y$ pixel, and is related to the power spectral density (PSD) of the sample's RI fluctuations after modulation by microscope transfer function [5]. As a statistical metric, Σ is sensitive to structural changes in the range of 20–300 nm, below the system's diffraction limit. However, it is not explicitly a structural metric and thus is not directly comparable to other nanoscale imaging techniques. Here, we outline and validate a method to relate Σ, a measured optical parameter, to D, a physical descriptor of nuclear organization, while considering the effect of chromatin volume concentration ϕ and genomic length N_f.

Within the nucleus, chromatin is the strongest contributor to the PWS signal, as most other macromolecules and physicochemical elements (i.e., ions) are outside the length-scale sensitivity of PWS. In order to establish a direct relationship between the chromatin packing scaling D from PWS spectral

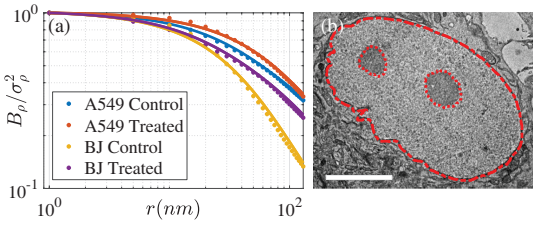

Fig. 1. B_ρ model (solid lines) fit to experimental ACFs of chromatin mass density computed from ChromTEM of nuclei. (b) ChromTEM image of a BJ nucleus with mask. Scale bar, 5 μm.

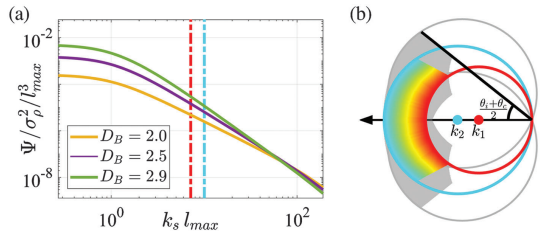

Fig. 2. (a) Normalized PSD Ψ is shown, where the dashed lines indicate the backscattered frequencies for visible light illumination. (b) Ewald representation of backscattered frequency space with NA_i of 0.55 and NA_c of 1.49. The colored region depicts wavelengths 500–700 nm for planar illumination, while the grayed region incorporates the response from the entire NA_i.

variance Σ, we first express Σ as a function of the mass-density autocorrelation function (ACF) shape parameter D_B, then convert D_B to D. The ACF of a purely fractal media is a power-law function with exponent proportional to packing scaling D as follows: $B_\rho \propto r^{D-3}$ [3]. However, a strict power-law approaches infinity at the origin, a behavior that is not physical, as the smallest structural units of chromatin are nucleotides. Additionally, the ACF of a PD gradually decays to zero. Thus, a modified power-law ACF was employed to include a lower and upper length scale limit, and allow for continuity and differentiability at all length scales [9,10]:

$$B_\rho(r) = A\,\sigma_\rho^2\, r^{D_B-3}\left[\Gamma\left(\frac{r}{l_{\max}}, 3-D_B\right) - \Gamma\left(\frac{r}{l_{\min}}, 3-D_B\right)\right], \tag{1}$$

where r is the spatial separation, and $A = \frac{D_B-3}{l_{\max}^{D_B-3} - l_{\min}^{D_B-3}}$ is the normalization term such that $B_\rho(r=0)$ is σ_ρ^2, the variance of mass density. $\Gamma(x, a)$ is the upper incomplete gamma function, and $l_{\min}$ and $l_{\max}$ characterize the lower and upper length scales of fractality, respectively. D_B is a model parameter that describes the shape of B_ρ and is related to D. This model for B_ρ was fit to experimentally measured ACFs from ChromTEM images of chromatin structure in lung adenocarcinoma A549 cells and differentiated BJ fibroblasts, and matched with marginal errors (median R^2 of 0.99 fit between 0–200 nm) (Fig. 1), demonstrating the flexibility of this model.

The scattering response of a medium can be determined by its PSD. Taking the 3D Fourier transform of $B_\rho(r)$, we obtain the PSD: $\Psi(k_s, D_B)$, a function of the scattering wavenumber in air k_s, shown in Fig. 2(a). Ewald representation for the PWS setup, Fig. 2(b), shows how the extended numerical aperture of a large collection (NA_c) and moderate illumination (NA_i) allows for high lateral resolution, while the spectrum enables differentiation between varying sample structures.

An ideal model has a direct correspondence between each physical descriptor and each model parameter. Within the fractal regime, the genomic size of chromatin, N_f, can be related to $l_{\max}$ by dividing the total volume by that of an elementary particle. Integrating the ACF over 3D space to obtain volume [3], we can compute N_f for a single domain as follows:

$$N_f = \frac{4\pi\int_0^\infty r^2\, B(r)\mathrm{d}r}{\frac{4}{3}\pi r_{\min}^3} = \frac{6(D_B-3)}{D_B}\frac{\left[1-\left(\frac{l_{\min}}{l_{\max}}\right)^{D_B}\right]}{\left[\left(\frac{l_{\min}}{l_{\max}}\right)^3 - \left(\frac{l_{\min}}{l_{\max}}\right)^{D_B}\right]}. \tag{2}$$

As N_f is monotonic with $l_{\max}$, Eq. (2) can be inverted numerically to compute the ACF as a function of N_f. Next, we relate the model parameter D_B to packing scaling D. The ACF slope was set to decay according to the packing scaling as follows:

$$D - 3 = \frac{\partial(\log B_\rho)}{\partial(\log r)}\Big|_{r=\frac{(l\max + l\min)}{60}}. \tag{3}$$

The D_B to D relationship, as determined from the fit to the slope in Eq. (3), is shown in Fig. 3(a), and is consistent for varying values of N_f and $l_{\min}$. Importantly, while D_B can take on any real value, D can physically take on values between 5/3 (self avoiding polymer) and 3 (space filling polymer).

Next, we utilize the relationship between spectral variance and the spatial ACF: $\Sigma^2 \propto [B_\rho \otimes T(r)]|_{r=0}$, denoted by the convolution (⊗) between the ACF and a smoothing function T, characterized by the microscope's NA and the source spectrum [5]. Since Σ^2 is linearly related to the ACF, a linear decomposition of the B_ρ results in a linear summation of Σ^2. B_ρ can be decomposed into a sum of weighted exponential functions:

$$B_\rho(r) = \int_{l_{\min}}^{l_{\max}} P(l_c, D_B)\, e^{-r/l_c}\,\mathrm{d}l_c. \tag{4}$$

Here, e^{-r/l_c} is a set of basis functions with varying l_c, the characteristic length. P, the probability distribution function for each length, is obtained by the normalized inverse Laplace transform of Eq. (4), given Eq. (1), as follows:

$$P(l_c, D_B) = l_c^{D_B-4}\frac{D_B-3}{l_{\max}^{D_B-3} - l_{\min}^{D_B-3}}. \tag{5}$$

Employing Parseval's theorem, Eq. (4) can be written in the spectral space with the same weighting function P. We thus obtain the relationship between spectral variance Σ^2 and D_B:

$$\Sigma^2(D_B) = \int_{l_{\min}}^{l_{\max}} P(l_c, D_B)\,\Sigma_e^2(l_c)\mathrm{d}l_c. \tag{6}$$

Σ_e^2 is the spectral variance from an exponential ACF with characteristic length l_c and has a closed-form solution [5]:

$$\Sigma_e^2(l_c) = \frac{2R^2\sigma_n^2}{\pi}\frac{l_c^3\, k^4\, L\, \mathrm{NA}_c^2}{(1+4k^2l_c^2)[1+k^2l_c^2(4+\mathrm{NA}_c^2)]} + R^2\sigma_n^2\left[1 - 1/\sqrt{1+(kl_c\mathrm{NA}_c)^2}\right]/4\quad, \tag{7}$$

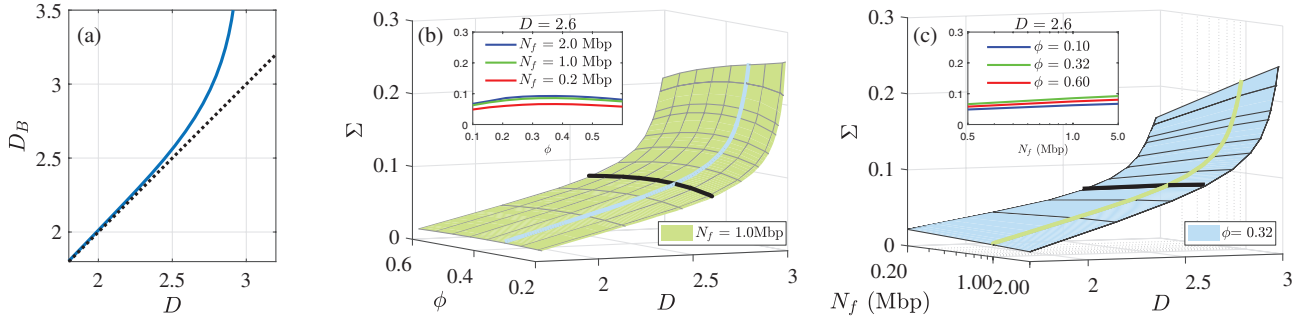

Fig. 3. (a) Model parameter D_B as it relates to D with the $y = x$ reference line shown. Surface plots showing (b) Σ versus D and ϕ; (c) Σ versus D and N_f; black lines denote the cross sections shown in respective insets.

where R is the product of the forward and reverse Fresnel transmission and reflection coefficients at the cell–glass interface, normalized by the reflectance of the glass–media interface:

$$R = \frac{4n_{\text{nucleus}}n_{\text{glass}}(n_{\text{glass}} - n_{\text{nucleus}})}{(n_{\text{glass}} + n_{\text{nucleus}})^3}\frac{(n_{\text{glass}} + n_{\text{media}})^2}{(n_{\text{glass}} - n_{\text{media}})^2}. \quad \textbf{(8)}$$

Additionally, k is the center wavelength in vacuum, L is the effective thickness of the sample limited by either the cell thickness or depth of field (DOF $= \pi n_{\text{oil}}/k\text{NA}_i^2$), and σ_n^2 is the variance of RI fluctuations within the nucleus.

Next, to estimate the RI of the nucleus n_{nucleus}, we consider the effect of chromatin density and mobile crowders (MCs, e.g., RNA polymerases, mRNAs) on scattering. The densities of these molecular components relate to n_{nucleus} through the Gladstone–Dale equation

$$n_{\text{nucleus}} = n_0 + \alpha\,\rho_C\,\phi + \alpha\,\rho_{\text{MC}}\,\phi_{\text{MC}}\,(1-\phi), \quad \textbf{(9)}$$

where $n_0 = 1.332$ is the RI of water, $\alpha = 0.18\frac{\text{cm}^3}{g}$ is the RI increment, and ρ_C and ρ_{MC} are the densities of chromatin and MCs, respectively. The chromatin volume concentration is ϕ, and the volume fraction of MCs in the nuclear space unoccupied by chromatin is denoted ϕ_{MC}. MCs consist of mediators, RNA polymerases, nucleosome remodelers, and histone modifiers, many of which are large protein complexes. The range of ρ_{MC} in the nucleus was estimated to be $1.3-1.7\frac{g}{\text{cm}^3}$, with larger proteins tending to have a lower density and larger volume fraction, thus we set $\rho_{\text{MC}} = 1.4\frac{g}{\text{cm}^3}$. We further estimated $\rho_C = 0.56\frac{g}{\text{cm}^3}$ by approximating the weight and total volume occupied by a single nucleosome and its linker DNA. Values of ϕ were kept within 0.12–0.55 [1]. Finally, we considered MCs to have a maximum volume concentration within the nucleus, $\phi_{\text{MC}} = 0.05$. Uncertainty propagation showed that $n_{\text{nucleus}} = 1.37 \pm 0.01$ resulted in a 7% change in Σ.

We estimated the standard deviation of RI fluctuations σ_n by assuming ϕ follows a binomial distribution:

$$\sigma_n = \sqrt{\phi(1-\phi)}\,[n_{\text{nucleus}}(\phi = 1) - n_{\text{nucleus}}(\phi = 0)]\,. \quad \textbf{(10)}$$

Then, we numerically calculated a series of $\Sigma(D_B)$ for varying D_B by first inputting physiologically relevant values for ϕ and N_f, and computing l_{max}, n_{nucleus}, and σ_n from Eqs. (2), (9), and (10), respectively. l_{min} was set to 1 nm, the radius of the fundamental structural unit of chromatin, the nucleotide base pair. These values were used in Eqs. (5) and (7) to compute P and Σ_e^2 as inputs to Eq. (6). Importantly, the relationship between Σ and D_B can be accurately represented by a linear approximation. For $\phi = 0.32$, $N_f = 1.0$ Mbp, $NA_i = 0.55$, and $\text{NA}_c = 1.49$, we obtain $\Sigma \approx 0.14(D_B - 1.45)$, with R^2 of 0.999.

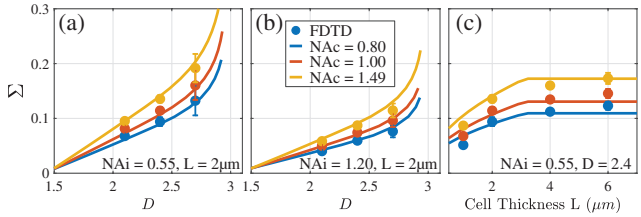

Fig. 4. Σ to D conversion (a), (b) for varying D and (c) cell thickness. FDTD and analytical results are shown for a wide range of system and media configurations.

Iterating through a range of D, we generated a numerical mapping of $\Sigma(D)$ as a function of ϕ and N_f, as shown in Figs. 3(b) and 3(c). The N_f values displayed (0.2–2 Mbp) encapsulate the interquartile range for PDs measured by ChromTEM. We note the primary contributor to changes in Σ are variations in D, even considering the extent of ϕ and N_f.

To validate this theoretical framework, we used Angora [11], software which implements finite difference time domain (FDTD) for microscopy modeling. We generated random media samples (five repetitions for each configuration) with dimensions 4 μm × 4 μm × L μm, resolution $\Delta x = 20$ nm, mean RI = 1.36, mounted on a glass slide (RI = 1.517) and immersed in cell media (RI = 1.337). The nuclear statistics were characterized by the ACF in Eq. (1), l_{min} was fixed to 1 nm, and $N_f = 1.0$ Mbp. We varied system parameters NA_i and NA_c and simulated an oil-immersion bright-field epi-illumination configuration, as per the experimental PWS system. The incident beam illuminated with wavelengths 500–700 nm, focused on the cell–glass interface, and backscattered images were measured in the far field. As consistent with PWS analysis, we first normalized the spectral cube to the reference, acquired from a cell-free simulation of glass–media interference. Next, we computed the pixel-by-pixel variance across wavelengths, and averaged Σ per simulation. FDTD results are plotted against theoretical derivations, and shown in Fig. 4. The analytical relationship here set $\sigma_n = 0.04$, as consistent with simulation.

Nuclear statistics from two cell lines were measured both by PWS and ChromTEM to show extensibility of the analytical approach: A549 and BJ cells untreated (control) or treated with

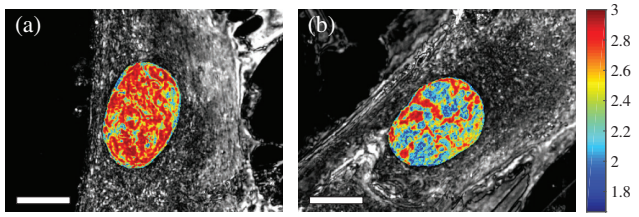

Fig. 5. PWS Dvalues of a BJ cell (a) before dexamethasone treatment and (b) 32 h afterwards. Scale bar, 10 μm.

a dose of 100 nM dexamethasone (Sigma-Aldrich, St. Louis, MO, D6645) were imaged after 12 h (A549) or 32 h (BJ) of treatment. Dexamethasone treatment has been demonstrated to alter whole-scale genome connectivity [12].

The PWS optical instrument is built on a commercial inverted microscope using a CCD coupled to a LCTF to perform hyperspectral imaging. Images were collected between 500 and 700 nm with 2 nm steps, and processed by normalizing by a reference measurement of the clear dish, convolving with a low pass filter, sinc(kDOF) to remove frequencies beyond the DOF, and computing the variance across wavelengths. Cells were cultured in 35 mm glass-bottom petri dishes until approximately 70% confluent, then imaged directly. A total of 300 A549 control, 323 A549 treated, 67 BJ control, and 100 treated BJ nuclei were accumulated in Σ measurements. PWS images of BJ cells after converting Σ to D are shown in Fig. 5.

ChromTEM samples were prepared by ChromEM staining protocol [1]. Following heavy metal staining, cells were dehydrated in ethanol, embedded in resin and cured for 48 h. Using an ultramicrotome, 50 nm thick resin sections were cut and deposited onto a copper 200 mesh grid with carbon/formvar film (EMS) and plasma cleaned. Each sample resulted in a 150 μm × 150 μm × 50 nm cross section of the cells, and imaged with 3 nm resolution. To process images, nuclear segmentation excluded background and nucleoli, as shown in Fig. 1(a). The 2D ACF of DNA density was computed, rotationally averaged, and D was fit with $B_\rho \propto r^{D-3}$ in the range of r between 50 and 100 nm. A total of 37 samples were acquired: eight A549 control, 12 A549 treated, five BJ control, and 12 BJ treated in the measurements of D.

Analytical and experimental results show a consistent trend, Fig. 6(a), where ChromTEM D and PWS Σ measurements from each cell population are plotted. While the true N_f of each cell population is unknown, the relationship between Σ and D is largely unaffected by N_f, and experimental results follow the theoretical mapping within physiological ranges for N_f. Using $N_f = 1$ Mbp and $\phi = 0.32$, we plot the D measured by both ChromTEM and PWS in Fig. 6(b) across all cell groups. Discrepancy in D may be due to the technical differences between the imaging techniques and cell groups.

We have theoretical framework to compute the physical chromatin packing scaling D, from optically measured interferometric spectral variance Σ. Validating it with FDTD simulations and ChromTEM imaging experiments, both with nanometer resolution, we found chromatin packing scaling

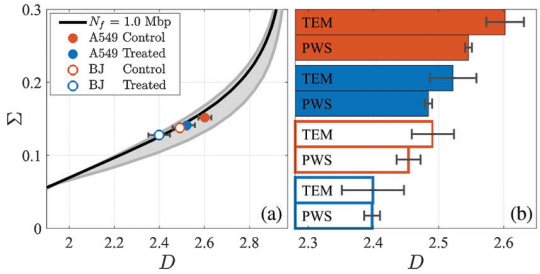

Fig. 6. (a) Σ versus D mapping, where gray lines denote N_f of 0.2–2.0 Mpb. Experimental measurements from two cell lines under two treatment conditions as measured by PWS (Σ) and ChromTEM (D) are shown. (b) With $N_f = 1$ Mbp and $\phi = 0.32$, PWS Σ were converted to D and are compared to ChromTEM. Error bars are standard error between average nuclear D.

D can be recovered. We believe this will enable interferometric imaging techniques to characterize tissue morphology for exploratory research, functional nano-sensing, and better characterization and detection of pathology.

Funding. National Institutes of Health (R01CA200064, R01CA225002, R01CA228272); National Science Foundation (EFMA-1830961).

Acknowledgment. An award of computer time was provided by the INCITE program. This research used resources of the Argonne Leadership Computing Facility, which is a DOE Office of Science User Facility supported under Contract DE-AC02-06CH11357 with guidance from Wei Jiang.

Disclosures. The authors declare no conflicts of interest.

REFERENCES

1. H. D. Ou, S. Phan, T. J. Deerinck, A. Thor, M. H. Ellisman, and C. C. O'Shea, Science **357**, eaag0025 (2017).
2. R. K. Wang, J. Mod. Opt. **47**, 103 (2000).
3. E. G. Iashina and S. V. Grigoriev, J. Exp. Theor. Phys. **129**, 455 (2019).
4. K. Metze, Expert. Rev. Mol. Diagn. **13**, 719 (2013).
5. L. Cherkezyan, D. Zhang, H. Subramanian, I. Capoglu, A. Taflove, and V. Backman, J. Biomed. Opt. **22**, 030901 (2017).
6. R. K. A. Virk, W. Wu, L. M. Almassalha, G. M. Bauer, Y. Li, D. VanDerway, J. Frederick, D. Zhang, A. Eshein, H. K. Roy, I. Szleifer, and V. Backman, Sci. Adv. **6**, eaax6232 (2020).
7. A. S. Hansen, C. Cattoglio, X. Darzacq, and R. Tjian, Nucleus **9**, 20 (2018).
8. T. Nozaki, R. Imai, M. Tanbo, R. Nagashima, S. Tamura, T. Tani, Y. Joti, M. Tomita, K. Hibino, M. T. Kanemaki, K. S. Wendt, Y. Okada, T. Nagai, and K. Maeshima, Mol. Cell **67**, 282 (2017).
9. M. Xu and R. R. Alfano, Opt. Lett. **30**, 3051 (2005).
10. C. J. R. Sheppard, Opt. Lett. **32**, 142 (2006).
11. I. R. Capoglu, A. Taflove, and V. Backman, IEEE Antennas Propag. Mag. **55**(4), 80 (2013).
12. A. M. D'Ippolito, I. C. McDowell, A. Barrera, L. K. Hong, S. M. Leichter, L. C. Bartelt, C. M. Vockley, W. H. Majoros, A. Safi, L. Song, C. A. Gersbach, G. E. Crawford, and T. E. Reddy, Cell Systems **7**, 146 (2018).